ELSEVIER

Earth and Planetary Science Letters 160 (1998) 257–271

EPSL

Revisiting the Lowrie–Fuller test: alternating field demagnetization characteristics of single-domain through multidomain glass–ceramic magnetite

Susan L. Halgedahl *

Department of Geology and Geophysics, University of Utah, Salt Lake City, UT 84112, USA

Received 2 September 1997; revised version received 21 April 1998; accepted 28 April 1998

Abstract

This paper reports the alternating field demagnetization characteristics of glass–ceramic magnetite assemblages carrying weak-field thermoremanent magnetization (TRM), weak-field anhysteretic remanent magnetization (ARM), and saturation remanence (J_{rs}). Average grain sizes vary from less than 0.1 μm to approximately 100 μm, and hysteresis parameters indicate that these assemblages encompass single-domain (SD) through truly multidomain (MD) behavior. In all assemblages, weak-field TRM and weak-field ARM are more stable to alternating field demagnetization than is (J_{rs}). This response is especially remarkable in the 100 μm assemblage, which otherwise displays truly MD behavior. Although the SD samples pass the Lowrie–Fuller test for SD behavior, calculations presented here show that populations of noninteracting, uniaxial SD grains should behave in just the opposite sense to that reported originally by Lowrie and Fuller. This discrepancy could indicate that SD, glass–ceramic magnetite populations are more affected by magnetic interactions than would be expected for magnetite crystals that nucleated individually from a silicate matrix. This interpretation is supported by the SD assemblages failing the 'Cisowski' test: that is, the curves for acquisition and AF demagnetization of (J_{rs}) intersect well below the 50% mark. However, a second and intriguing explanation of the SD-like results obtained from all samples is that alternating field demagnetization characteristics reflect a strong dependence of local energy minimum domain state, and its associated stability, on the state of magnetization.

Keywords: magnetite; glass materials; ceramic materials; alternating field demagnetization

1. Introduction

To better understand the origins of natural remanent magnetization (NRM) in rocks, rock magnetists and paleomagnetists have devoted much effort toward the synthesis and study of artificial samples, as well as toward devising tests to elucidate the domain state and type of remanence associated with the dominant magnetic carriers. To date, the glass–ceramic (GC) method is thought to yield the closest synthetic analogues of the magnetic minerals in certain igneous rocks [1–3]. For this reason, rock magnetic characterization of GC assemblages can provide key insights into many types of natural samples. A fundamental step toward such characterization is to deter-

* Tel.: +1 (801) 581-7162; Fax: +1 (801) 581-7065; E-mail: shalg@mines.utah.edu

0012-821X/98/$19.00
PII S0012-821X(98)00085-5

mine how various aspects of magnetic behavior, such as hysteresis parameters, vary with average grain size. These grain-size variations are not functions of composition alone, but are quite sensitive to the mode of synthesis. Worm [1] and Worm and Markert [3] reported the grain-size dependence of hysteresis parameters B_c (coercive force) and J_{rs}/J_s (ratio of saturation remanence to saturation magnetization) in assemblages of GC magnetite, whose average sizes ranged from approximately 100 μm to about 0.03 μm. Their samples encompassed the truly multidomain (MD) through the single-domain (SD) states, and B_c varied from only a few mT in the most MD assemblages to several tens of mT in assemblages consisting largely of stable SD grains. The recent data compilation of Hunt et al. [4] shows that for a given average grain size, B_c and J_{rs}/J_s are much higher in GC assemblages than in magnetite populations grown synthetically without a parent matrix, such as hydrothermally at elevated temperature [5], at room temperature in an aqueous medium [6], or through reduction of fine-grained hematite [7]. Almost certainly, these marked differences reflect the high levels of residual microstress that GC samples acquire during synthesis at high temperature. On the other hand, at any given grain size both J_{rs}/J_s and B_c in GC samples are lower than in dispersions of crushed grains [4]. Thus hysteresis and other rock magnetic properties depend not only on composition, grain size, and magnetic domain state, but on stress–strain history and the defect densities that result. Analogous differences are expected among magnetite populations present in rocks of very different provenances.

Although hysteresis parameters contain key information about magnetic domain state, internal anisotropy energies, and wall–defect interactions, the Lowrie–Fuller test [8] often has been used to assess domain state and/or the type of NRM associated with the principal remanence carriers in rocks. In its original form, this test is stated as follows. If weak-field thermoremanent magnetization (TRM), normalized to its initial value, is less stable to alternating field demagnetization (AFD) than is the normalized saturation remanent magnetization acquired at room temperature, then the dominant magnetic carriers are thought to be in a truly MD state. If the opposite is true, then the carriers are thought to be SD. Lowrie and Fuller based their test on experimental data from two very different suites of samples: (1) a dispersion of fine-grained (0.1 μm), presumably SD magnetite studied earlier by Rimbert [9]; and (2) three samples known to be in a truly MD state: polycrystalline magnetite ore, a rod made from a single crystal of magnetite, and a dispersion of large (≅250 μm) grains of magnetite. Subsequently, a modified version of the test was introduced by Johnson et al. [10], who showed that anhysteretic remanent magnetization (ARM) acquired in a weak biasing field is a reasonable analogue of weak-field TRM. ARM has the distinct advantage of being induced at room temperature, so that chemical alteration due to heating is avoided.

To better understand the Lowrie–Fuller test, Bailey and Dunlop [11] and Dunlop [12] studied AFD behavior in a wide variety of igneous rocks and in synthetic samples of crushed, dispersed magnetite that encompassed pseudosingle-domain (PSD) to truly MD hysteresis behavior. Most significantly, Bailey and Dunlop's experiments showed that their finest-grained, PSD assemblages (≅2–4 μm in size) responded in a 'SD-like' manner by the original Lowrie–Fuller criterion. According to Bailey and Dunlop's models, a 'SD-like' Lowrie–Fuller response reflects the combined effects of the internal demagnetizing field and a superexponential distribution of microcoercivities on the stability of domain walls; in contrast, they predicted that a subexponential microcoercivity spectrum would yield a 'MD-like' Lowrie–Fuller test. A more general model by Xu and Dunlop [13] shows that the Lowrie–Fuller response of a two-domain grain depends on the number of dislocations that effectively pin the wall.

The Lowrie–Fuller behavior of GC magnetite has not been reported previously. Therefore, we have studied AFD responses of weak-field TRM, weak-field ARM, and (J_{rs}) carried by GC magnetite assemblages dominated by SD through truly MD grains. These samples were synthesized originally by H.-Ü. Worm and were kindly donated to the author of this paper by W. Williams, who investigated viscous behavior of companion samples [14]. The low-temperature behavior of the samples studied here has been described earlier by Halgedahl and Jarrard [15].

2. Samples and experimental methods

2.1. Sample characteristics

Samples from five batches of GC magnetite were studied. According to Worm [1] and Williams [14], average grain sizes in the five batches are ≤0.1 μm, ≅0.1–0.3 μm, 1.5 μm, 7 μm, and 100 μm, respectively.

In the present study, grain sizes and hysteresis parameters were determined for samples from each batch. Size distributions were obtained in a scanning electron microscope (SEM), rather than in a transmission electron microscope (TEM), in order to avoid destroying much of the limited amount of available material when making the many ultrathin sections required for meaningful grain-size analyses in TEM. First, using backscattered electron mode, magnetite particles were located on polished surfaces. Next, using secondary electron mode, magnetite grains were photographed to obtain more accurate size determinations than backscattered electrons would provide. The two largest-grained assemblages also were examined under high magnification to detect whether or not significant populations of submicron grains were present.

Hysteresis parameters were obtained with an alternating gradient field magnetometer (AGFM; Princeton Measurements Corporation). A maximum field (B_{max}) of 1.3 T (H_{max} = 13 kOe, cgs) was used in all runs. The diamagnetic and/or paramagnetic contributions from the sample probe and/or from the sample itself were removed with a slope-correction algorithm. All samples yielded loops with a 'normal' shape, with no sign of wasp-waistedness.

Average grain sizes, J_{rs}/J_s, and B_c are listed in Table 1 for samples from the five batches. The five grain-size distributions are shown as histograms in Appendix A. Average sizes obtained in this work are very similar to those reported by Worm [1] and Williams [14]. Note that the <0.1 μm assemblage contains some elongate magnetite grains arrayed in a chain-like fashion. Because submicron magnetite particles were observed so rarely in the ≅100 μm assemblage, they were not included in the histogram in order to maximize resolution on the plot near 100 μm. Perhaps the most notable difference between average grain size determined here and that published earlier [1,14] was found in the ≅0.2 μm assemblage. Although not fully understood, this difference could reflect real variations of average size among the particular magnetite clusters in the subsamples studied by different workers. Also, this difference could result from grains' true diameters not always being exposed on a polished surface. Note that, in all samples, this latter effect would broaden the apparent grain-size distribution at sizes below the true mean.

Table 1
Grain size and hysteresis parameters

Average grain size, μm			J_{rs}/J_s (this study)	B_c, mT [a] (this study)
This study	Worm [1]	Williams [14]		
≅0.06–0.1 [b]	<0.1 [b]	≅0.1 [b]	0.414	44.7
			0.438	47.1
			0.432	47.1
≅0.2	<0.1	≅0.3	0.389	41.9
			0.382	42.2
			0.371	43.0
≅1.5	1.5	1.5	0.087	11.4
			0.098	12.0
			0.174	18.6
≅7	7	7	0.033	4.09
			0.032	3.94
			0.033	3.92
			0.036	4.53
≅100	100	100	0.019	1.92
			0.018	1.85

[a] 1 mT (B: SI) equivalent to 10 Oe (H: cgs).
[b] Grains somewhat elongate, sometimes arrayed in chains.

Owing to the resolution limit of the SEM used here (about 0.05 μm) and to the nonuniform distribution of particles in the two finest-grained assemblages, the size distributions obtained from these two assemblages almost certainly are biased toward the coarser ends of their spectra. Although, in these two samples, magnetite grains smaller than about ≅0.075 μm could be detected, their relative numbers and sizes are very approximate (Appendix A). For this reason we have designated the average grain sizes of these two finest-grained assemblages as <0.1 μm and ≅0.2 μm, respectively. Despite these uncertainties, it is unlikely that the <0.1 μm assemblage contains a large percentage of magnetite grains substantially smaller than about 0.05 μm, since such an ultrafine population could exert a strong, superpara-

magnetic influence and could produce wasp-waisted hysteresis loops. Such loops were not observed.

In Fig. 1, the grain-size dependences of J_{rs}/J_s and B_c obtained here are compared to those of Worm, who used a vibrating sample magnetometer (table 6.1 in Ref. [1]). Because the magnetites in two of Worm's finest-grained assemblages were described only as being smaller than 0.1 μm [1], their hysteresis parameters have been plotted at a grain size of 0.1 μm in Fig. 1. Overall, there is good consistency among the hysteresis parameters of companion samples measured here from each batch. Clearly, the present results agree well with those reported by Worm [1].

The most physically significant departures between the present hysteresis results and those of Worm [1] are exhibited by samples dominated by submicron magnetite. For example, Worm [1] obtained $J_{rs}/J_s = 0.5$ for one of his samples described as containing <0.1 μm magnetite. In contrast, for a companion sample we obtained J_{rs}/J_s =0.41–0.44. Note, however, that Worm [1] used $B_{max} = 0.8$ T (8 kOe) to study hysteresis behavior of this particular assemblage (see fig. 6.2 in Ref. [1]). When the same B_{max} was used in the AGFM, we also obtained $J_{rs}/J_s \cong 0.5$. Increasing B_{max} above 0.8 T had little effect on the intensity of (J_{rs}), however. Quite possibly, 0.8 T is sufficiently strong to reverse all of the particle's moments and thus yields an accurate value of (J_{rs}) for this assemblage. However, 0.8 T may be insufficient to completely align the moments of the highest-coercivity particles at the top of the hysteresis loop. If so, then raising B_{max} would lower the resultant value of J_{rs}/J_s. Also, this difference could reflect the two different methods used to correct for dia- and/or paramagnetism. Nevertheless, the ratio J_{rs}/J_s appears to peak when the average grain size is near 0.1 μm [1] (Fig. 1a). In much smaller grains (≅0.03 μm), J_{rs}/J_s is considerably less than 0.5 due to the effects of superparamagnetism [1]. Therefore, it is probable that the <0.1 μm assemblage studied here contains a very large percentage of uniaxial, SD grains.

2.2. Experiments

Weak-field TRMs were induced by cooling each sample in air from 590°C in a field of 50 μT (0.5 Oe, cgs). These and previous experiments with companion samples show that heating in air to the Curie point of magnetite (≅580°C) has little effect on magnetic properties, such as hysteresis parameters or viscosity coefficients [14,16]. Evidently, the silicate matrix protects the magnetite grains from heating-induced alteration. Next, ARMs were given in a peak AF of 0.1 T (the maximum AF provided by the available ARM equipment), upon which a 50 μT biasing field was superimposed. Isothermal remanent magnetization (J_r) was given in increasingly stronger fields, in order to obtain the J_r-acquisition curve. Saturation remanences were given through exposure to a 0.57 T field.

After each of the three principal types of remanence was acquired, the samples were AF demagnetized along one axis in a stepwise manner to a maximum peak AF of at least 0.1 T, or until directional consistency of the magnetization was lost. In all cases, the axis of demagnetization was collinear with remanence. Remanences were measured in a 3-axis cryogenic magnetometer.

3. Results

Normalized AFD curves of weak-field TRM, (J_{rs}), and weak-field ARM for all five assemblages are shown in Fig. 2. As expected, all three principal types of remanence generally grow less stable to AFD as grain size increases.

For each sample, the AFD curves of TRM and (J_{rs}) are compared to each other in Fig. 3a–e. Also shown are portions of each J_r-acquisition curve. In all five samples, (J_{rs}) is less stable to AFD than is weak-field TRM. Furthermore, in all samples the J_r-acquisition curve and the AFD curve of (J_{rs}) intersect well below 0.5.

In the 7 and 100 μm assemblages, the normalized AFD curves of ARM and TRM are very similar across their entire coercivity spectra (Fig. 3f). In the <0.1, ≅0.2, and 1.5 μm assemblages, however, the curves for ARM and TRM are similar only to peak AFs of about 70–90 mT (Fig. 2); in stronger peak fields, ARM is softer than TRM. Almost certainly, this difference occurs because the maximum AF (0.1 T) available for ARM acquisition is insufficient to fully reverse and saturate the most highly coercive grains in these three, finer-grained samples.

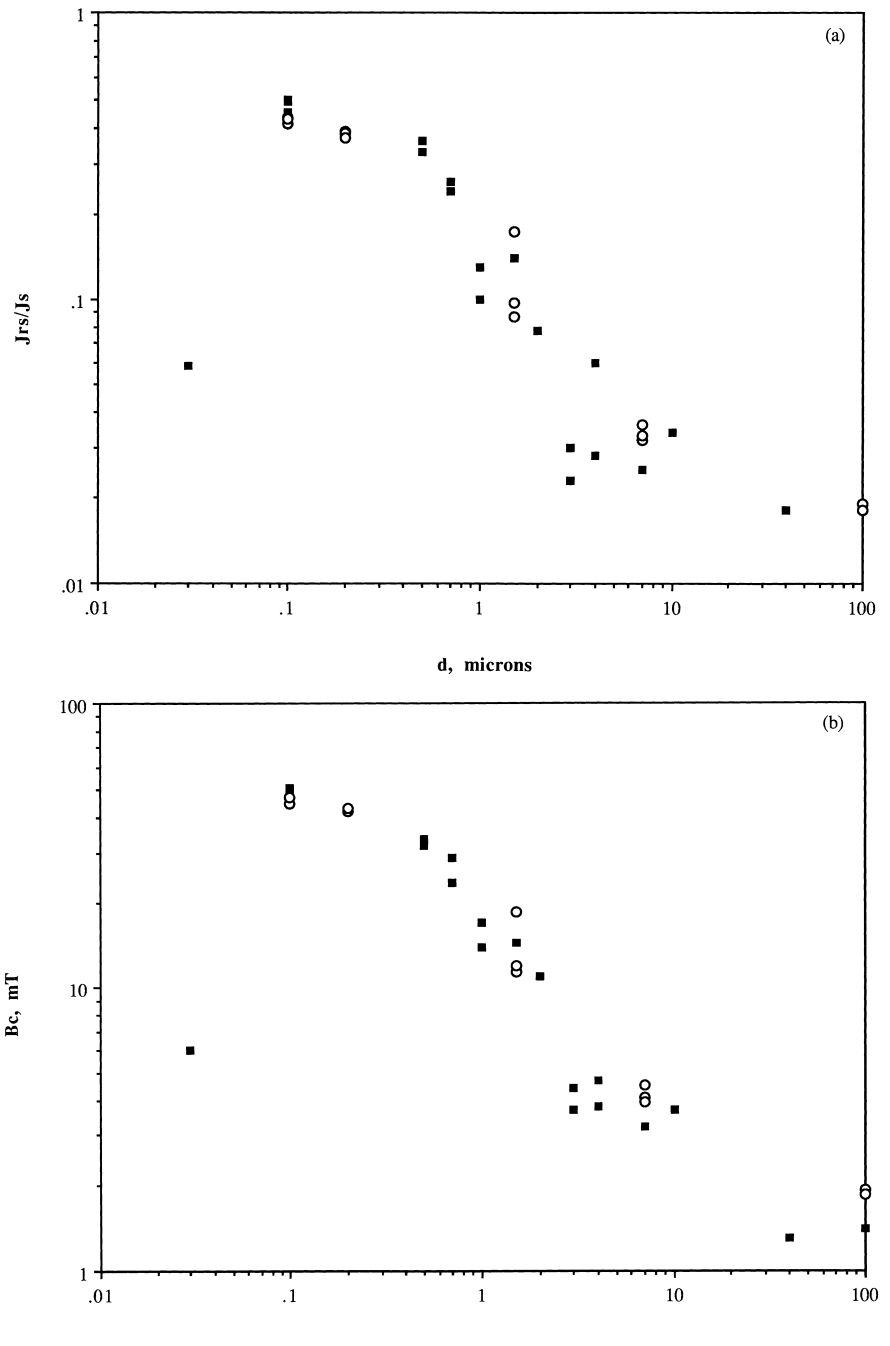

Fig. 1. (a) The ratio saturation remanence/saturation moment (J_{rs}/J_s) and (b) coercive force (B_c) plotted as functions of grain size for glass–ceramic magnetite (GC) assemblages. Squares, data of Worm [1]; circles, this study.

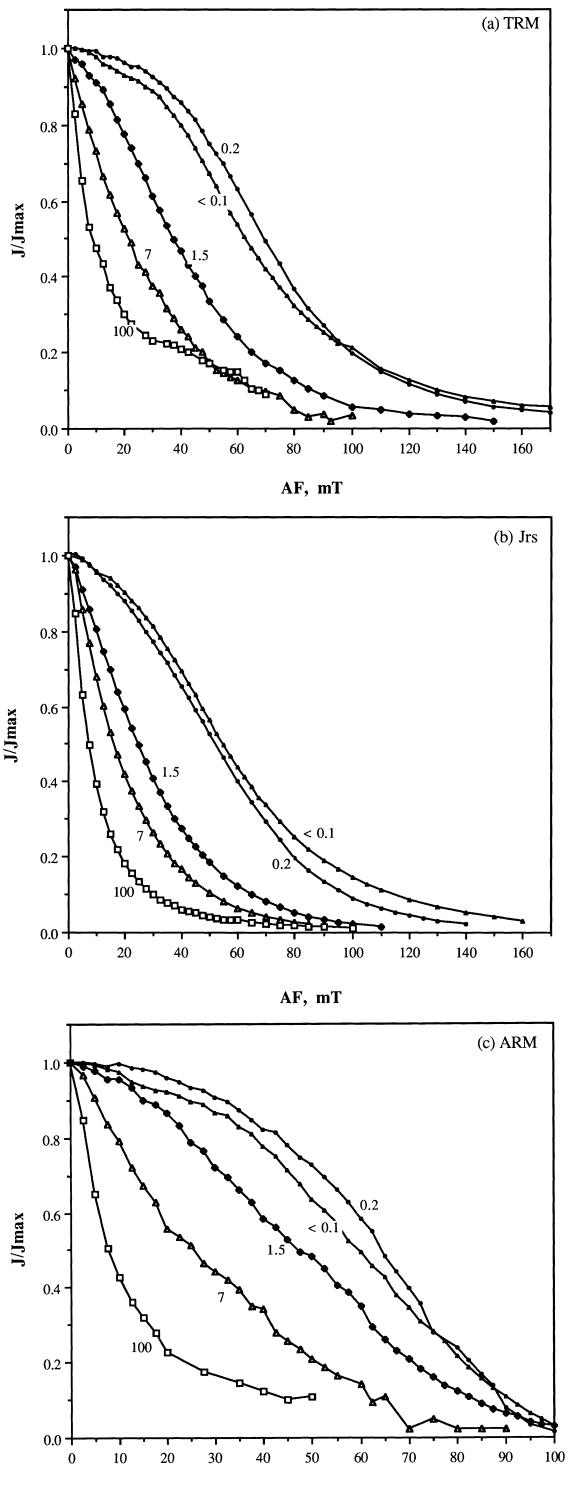

Consequently, in these particular experiments the AFD curves of weak-field TRMs are considered to be of more fundamental significance than those of weak-field ARMs.

4. Discussion: PSD through truly MD assemblages

Two notable features emerge from this suite of data: curve shape and the relative AF stabilities of the different types of remanence. Grain size has a striking impact on the shapes of these curves. The two submicron assemblages yield curves which are strongly concave downward to AFs approximately equal to the median destructive field (e.g. ≅50 mT in these two samples). In contrast, curves of the 7 and 100 μm assemblages are strongly concave upward across most of their coercivity spectra, until the curves flatten out in high AFs (Figs. 2 and 3). The transition in curve shape occurs in the PSD range near 1 μm, as exemplified by the 1.5 μm assemblage. In this sample, AFD curves for ARM and TRM are only slightly concave downward in AFs less than about 20 mT; in contrast, the curve for (J_{rs}) is decidedly MD-like in shape. Bailey and Dunlop [11] obtained a very similar result from sized dispersions of crushed magnetite. In their samples, they concluded that this change in curve shape marked the transition from PSD to truly MD behavior.

Fig. 2. Normalized alternating field demagnetization (AFD) curves of: (a) weak-field (50 μT) thermoremanent magnetization (TRM); (b) saturation remanence (J_{rs}), and (c) weak-field (50 μT) ARM carried by the five GC magnetite assemblages studied here. The number adjacent to each curve represents the assemblage's average grain size, in μm (1 mT, SI, of peak AF is equivalent to 10 Oe, cgs).

Fig. 3. (a–e) Normalized AFD curves of weak-field TRM (circles) and J_{rs} (crosses) for each of the five GC magnetite assemblages. Also shown is part of the J_{rs}-acquisition curve for each sample (triangles). Average grain sizes are indicated on each figure. (f) Normalized AFD curves of weak-field TRM (circles) and weak-field ARM (dots) for the ≅7 μm assemblage, showing that TRM and ARM have very similar AFD spectra in this sample.

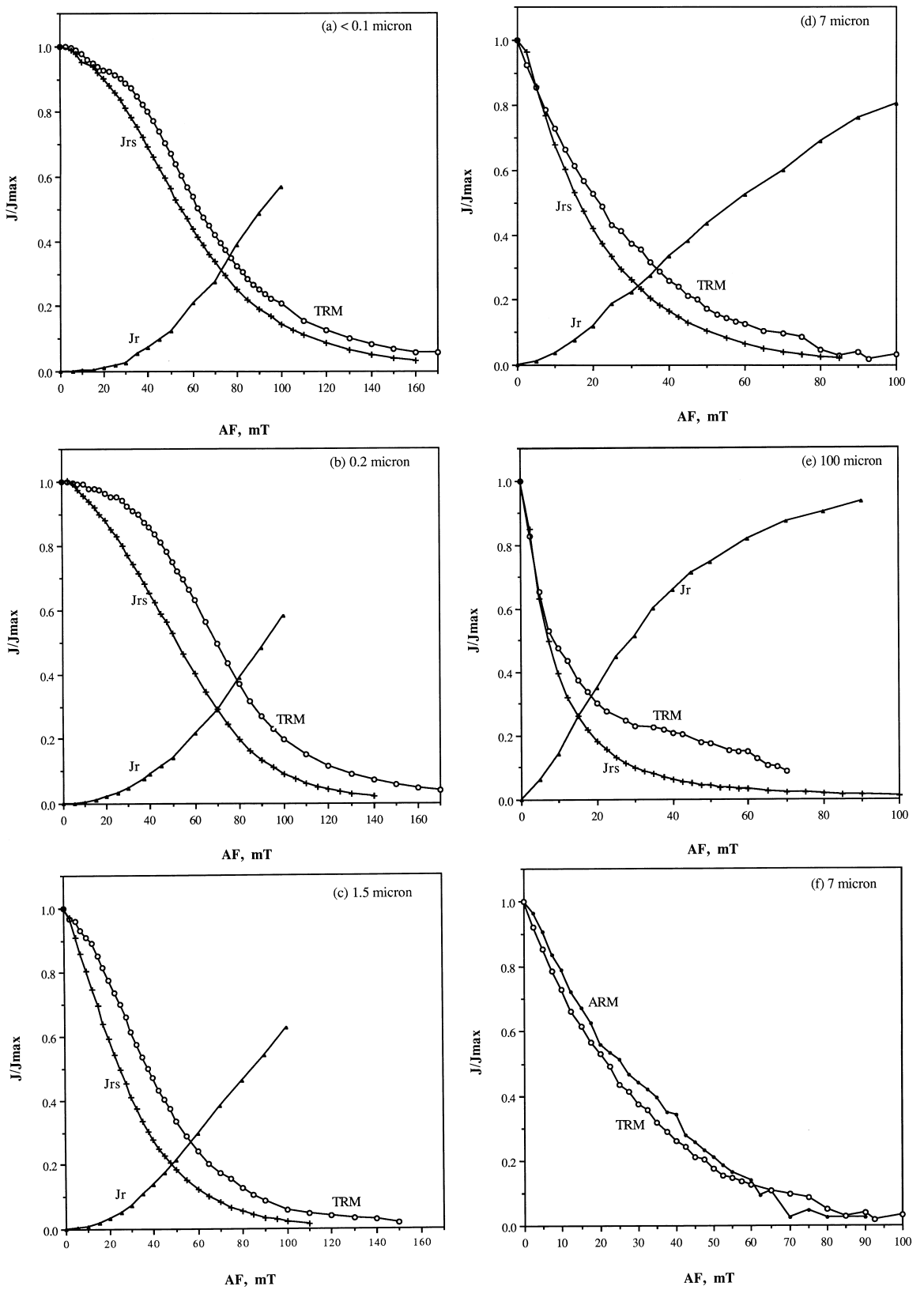
(a) < 0.1 micron
(b) 0.2 micron
(c) 1.5 micron
(d) 7 micron
(e) 100 micron
(f) 7 micron
J/Jmax
AF, mT
Jrs
Jr
TRM
ARM

In terms of relative AF stabilities, all of the GC magnetites studied here give SD-like Lowrie–Fuller tests across most of their coercivity spectra, regardless of grain size or curve shape. According to a model developed by Xu and Dunlop for two-domain grains of magnetite [13], AF stability depends both on the type of remanence and on the number of dislocations that a wall intersects. Consequently, whether or not an assemblage yields a SD-like or a MD-like Lowrie–Fuller test depends on both grain size — i.e. wall area — and the dislocation density. For example, a SD-like Lowrie–Fuller response can ensue when relatively few dislocations intersect a wall, as may occur in very small particles. But the same dislocation density can produce a MD-like Lowrie–Fuller response in very large grains, if their walls intersect an extremely large number of dislocations.

Xu and Dunlop's model is supported partly by results of Heider et al. [17], who found that the median destructive field of TRM exceeded that of (J_{rs}) in dispersions of hydrothermally grown magnetite grains up to approximately 100 μm in average grain diameter; above this size the opposite relation was found. Because this method of synthesis is thought to produce a very low density of dislocations, Xu and Dunlop's model predicts that even large magnetite particles of this type could give SD-like Lowrie–Fuller trends.

In contrast to hydrothermally grown magnetites, populations of crushed magnetite give SD-like Lowrie–Fuller trends only to about 10 μm; in larger particles, MD-like Lowrie–Fuller trends are obtained [11]. By Xu and Dunlop's model [13], such results would indicate that crushed magnetites have high dislocation densities. This conclusion is not surprising, because crushing undoubtedly causes severe plastic deformation.

Thus, results from the 100 μm assemblage are surprising in two ways. First, this assemblage exhibits truly MD behavior in its hysteresis parameters. Since submicron particles are very rare in this sample, it is highly improbable that its AFD behavior is attributable to a large population of extremely small, SD grains. Second, when the 100 μm results are viewed in terms of Xu and Dunlop's model [13], one would conclude that dislocation densities in 100 μm, GC magnetites are comparable to those in hydrothermally grown magnetite particles of commensurate size. Certainly, this conclusion is erroneous. Because the thermal expansion coefficient of magnetite is different from that of the silicate matrix, one would predict that GC magnetite grains acquire high internal stresses during synthesis, and that these stresses are associated with a high dislocation density (e.g. $\gg 10^{12}/m^2$). This expectation is supported by $\cong 1$ μm- to 100 μm-sized GC magnetites having B_c values which are about ten times higher than those of hydrothermally grown magnetites of comparable size [4].

Therefore, Xu and Dunlop's model may be too simple to explain the Lowrie–Fuller responses of different types of magnetite assemblages that span a wide range of grain sizes and internal stress states. In their model, Xu and Dunlop consider only the effect of line defects [13]. But on the bases of theory and the observed temperature dependence of B_c, Moskowitz [18] concluded that negative dislocation dipoles could account for coercivities observed in hydrothermally grown magnetites. In contrast, a population of both positive and negative dislocation dipoles could explain coercivities in GC magnetite samples [18]. Resolution of the conflict between the present results and Xu and Dunlop's model requires future experimental tests with samples whose defects have been well-characterized.

Clearly, the Lowrie–Fuller test is neither diagnostic of domain state, when the type of remanence is known, nor of the type of remanence, when the domain state is known independently from parameters such as hysteresis ratios.

5. SD behavior: experiment versus theory

It is generally thought that our understanding of homogeneously magnetized, SD grains far exceeds our understanding of PSD or truly MD grains. Not only do particles in the latter two states contain domain walls, but they may occupy a variety of local energy minimum, or LEM, domain states [19]. What is not widely recognized is that the AFD responses of SD grains conflict with traditional Néel theory [20,21]. In a very brief proof, Schmidt [22] showed that SD assemblages should exhibit Lowrie–Fuller trends which are opposite in sense to those obtained experimentally. An expanded and more general ver-

sion of this proof is presented below, based on Néel's theory of weak-field TRM in SD grains [20,21]. For several simple cases, AFD curves of weak-field TRM and (J_{rs}) are calculated for aligned, SD assemblages.

5.1. Model for weak-field TRM

In this model we assume that an assemblage of uniaxial, noninteracting, SD particles of magnetite satisfies the following simplifying conditions.

(1) All easy axes of magnetization are collinear with each other, with the TRM acquisition field b_{ex}, with the (J_{rs})-inducing field, and with AFs subsequently applied during demagnetization.

(2) At temperatures below the Curie point, particles are homogeneously magnetized and reverse their moments through coherent rotation.

(3) Particles are controlled by a strong uniaxial anisotropy caused by either shape or stress; thus, cubic magnetocrystalline anisotropy is neglected at all temperatures.

(4) Grain volume v is independent of B_{co}, where B_{co} is the intrinsic, critical field needed to irreversibly flip a grain's magnetic moment at room temperature T_o (= 293 K).

(5) Because v and B_{co} are independent of each other, the probability that a grain has volume v, within the differential volume element dv, is given by $P\,dv$, where P is the normalized probability density with respect to v and where P is solely a function of v. Likewise, the probability that a grain has a critical field B_{co}, within the differential element dB_{co}, is given by $Q\,dB_{co}$, where Q is the normalized probability density with respect to B_{co} and where Q is solely a function of B_{co}.

(6) Grain volume v ranges from a minimum of v_{min} to a maximum of v_{max}; similarly, B_{co} ranges from $B_{co,min}$ to $B_{co,max}$.

(7) In all grains both v and B_{co} are sufficiently large so that the experimental field necessary for reversal is unaffected by thermal fluctuations at T_o.

(8) At the TRM blocking temperature, the grains' intrinsic coercivities are much larger than b_{ex}; consequently, TRM $\propto b_{ex}$.

Following Néel's theory [20,21], TRM is blocked at a temperature T_b where the relaxation time $\tau \cong 60$ s $\cong 10^{-9}$ s $[\exp(\Delta E/kT)]_{at\,T_b}$. Here, ΔE is the energy barrier to reversal, k is Boltzmann's constant, and T is absolute temperature. At $T = T_b$, $\Delta E/kT \cong 25$. Although ΔE actually is a function of b_{ex} [20,21], we assume that b_{ex} is sufficiently weak to have negligible effect on ΔE at temperatures near T_b. Because the grains are assumed to be uniaxial, then near T_b the energy barrier $\Delta E \cong K_u v$, where K_u is the uniaxial anisotropy energy density due either to shape or stress at T. After expressing ΔE as a function of a grain's critical field B_c at T (see Appendix B), then near T_b shape energy gives $\Delta E_{near\,T_b}/kT \cong [M_{so} m^2 B_{co} v]/[2kT]$. In magnetite, stress energy gives $\Delta E_{near\,T_b}/kT \cong [M_{so} m^{2.25\,to\,3} B_{co} v]/[2kT]$. Here, $m = M_s/M_{so}$, where M_s is spontaneous magnetization at T and M_{so} is spontaneous magnetization at T_o. For magnetite, the temperature dependence of m and the m-dependences of B_c for shape and stress anisotropy are given in Appendix B [23–25].

If an assemblage contains N_{tot} particles, then the total TRM is:

$$\mathrm{TRM_{tot}} = N_{tot} M_{so} \int_{v_{min}}^{v_{max}} \int_{B_{co,min}}^{B_{co,max}} \left\{ v \tanh[M_{so} m_b v b_{ex}] \times (kT_b)^{-1} \right\} P\,Q\,dv\,dB_{co} \quad (1)$$

where the subscript 'b' indicates that a parameter is evaluated at T_b. When the argument in the hyperbolic tangent term is small (e.g. <0.5), as would occur in a weak field, then:

$$\mathrm{TRM_{tot}} \approx N_{tot} M_{so} \int_{v_{min}}^{v_{max}} \int_{B_{co,min}}^{B_{co,max}} \left\{ v\,[M_{so} m_b v b_{ex}] \times (kT_b)^{-1} \right\} P\,Q\,dv\,dB_{co} \quad (2)$$

5.2. Saturation remanent magnetization (J_{rs}) at room temperature

The total (J_{rs}) is:

$$J_{rs} = N_{tot} M_{so} \int_{v_{min}}^{v_{max}} P\,v\,dv \quad (3)$$

5.3. AF demagnetization

Let both $\mathrm{TRM_{tot}}$ and (J_{rs}) be demagnetized in an alternating field of peak intensity B along the axis of remanence. After surviving remanences are

normalized with respect to initial remanences, then one obtains:

$$\mathrm{TRM_{left}/TRM_{tot}} = 1 - \frac{\int_{v_{min}}^{v_{max}} \int_{B_{co,min}}^{B} \{v\,[M_{so} m_b v b_{ex}]\,/\,(T_b)\}\,P\,Q\,\mathrm{d}v\,\mathrm{d}B_{co}}{\int_{v_{min}}^{v_{max}} \int_{B_{co,min}}^{B_{co,max}} \{v\,[M_{so} m_b v b_{ex}]\,/\,(T_b)\}\,P\,Q\,\mathrm{d}v\,\mathrm{d}B_{co}} \quad (4)$$

Likewise,

$$J_{r,left}/J_{rs} = 1 - \frac{\int_{v_{min}}^{v_{max}} \int_{B_{co,min}}^{B} P\,v\,Q\,\mathrm{d}v\,\mathrm{d}B_{co}}{\int_{v_{min}}^{v_{max}} \int_{B_{co,min}}^{B_{co,max}} P\,v\,Q\,\mathrm{d}v\,\mathrm{d}B_{co}} \quad (5)$$

By the relations above, 'passage' of the Lowrie–Fuller test for SD behavior depends on weak-field TRM stemming mainly from the high-coercivity fraction and on (J_{rs}) stemming mainly from the low-coercivity fraction. The term $m_b v/T_b$ acts as a TRM weighting factor. Does this factor give most weight to high-coercivity or to low-coercivity grains? We have calculated $m_b v/T_b$ for several different grain volumes and a range critical fields arising either from uniaxial stress or shape in magnetite. For the case of stress, it is assumed that the magnetostriction constant $\lambda \propto m^3$ [23–25] and that $B_{co,max} = 200$ mT (see Appendix B). In Fig. 4a, $m_b v/T_b$ is plotted as a function of B_{co} controlled by stress and for grains of two different volumes. For any given v, this weighting factor is highest for the lowest coercivities and lowest for the highest coercivities. This follows naturally from the expression for τ at T_b: for a fixed v, as B_{co} increases, then the ratio m_b/T_b must decrease. Analogous trends are obtained for shape-dominated grains.

Fig. 4a demonstrates clearly that for any distributions P and Q, it is the low-coercivity grains that contribute most, and the high-coercivity grains that contribute least, to the total TRM (Eq. 2). Thus for any given AFD level above $B_{co,min}$, the model predicts that $\mathrm{TRM_{left}/TRM_{tot}} < J_{r,left}/J_{rs}$. This inequality holds regardless of the specific volume distribution or coercivity distribution of the assemblage under consideration.

Next, normalized AFD curves have been calculated for weak-field TRM and (J_{rs}) for grains controlled by uniaxial shape anisotropy and of volume $v = (5 \times 10^{-8}\ \mathrm{m})^3$ (see Appendix B). To simplify these calculations and to avoid weighting the coer-

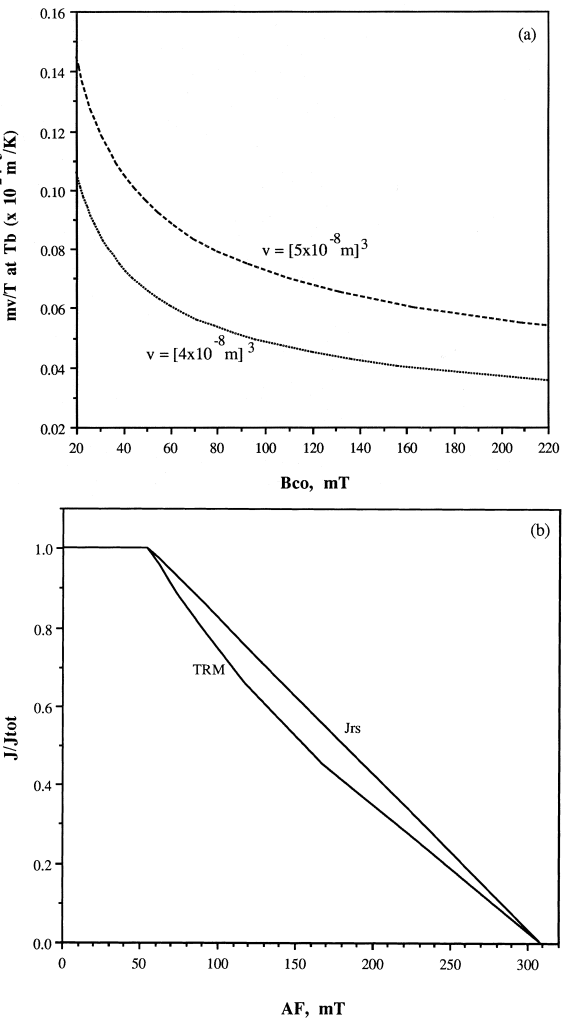

Fig. 4. (a) The TRM weighting factor mv/T (at T_b) plotted as a function of room-temperature critical field, B_{co}, for two assemblages of homogeneously magnetized, aligned, noninteracting, single-domain (SD) magnetite grains dominated by uniaxial stress. Units of mv/T: 10^{-24} m^3/K. In the first assemblage, all grains have volume $v = [5 \times 10^{-8}\ \mathrm{m}]^3$ (top curve). In the second assemblage, all grains have volume $v = [4 \times 10^{-8}\ \mathrm{m}]^3$ (bottom curve). Here, m is reduced spontaneous magnetization, M_s/M_{so}, calculated at the TRM blocking temperature T_b and M_{so} is spontaneous magnetization at room temperature T_o (see text and Appendix B). Note that mv/T decreases as B_{co} increases. Although not shown, the two curves continue to rise steeply as B_{co} decreases toward smaller values. (b) Normalized AFD curves of weak-field TRM (bottom curve) and J_{rs} (top curve) calculated for a population of homogeneously magnetized, uniaxial, aligned, noninteracting, SD grains of magnetite dominated by shape anisotropy and of volume $v = [5 \times 10^{-8}\ \mathrm{m}]^3$. In this model it is assumed that critical fields between $B_{co,min} = 56.2$ mT and $B_{co,max} = 301.6$ mT are equally probable (see Appendix B).

civity spectrum in favor of either high-coercivity or low-coercivity grains, Q is assumed to be a boxcar function from $B_{co,min}$ to $B_{co,max}$ and zero outside this range. Calculated curves are shown in Fig. 4b. As predicted, (J_{rs}) is more stable to AFD than is TRM. By this model, assemblages of noninteracting, uniaxial SD grains should 'fail' the Lowrie–Fuller test.

5.4. SD results versus predictions

Perhaps the three best criteria for testing whether SD assemblages fulfill the assumptions of the model above are: (1) a ratio of J_{rs}/J_s very near or equal to 0.5; (2) a ratio of remanent coercivity to coercive force (B_{cr}/B_c) only slightly greater than 1.0; (3) a positive 'Cisowski' test, according to which the normalized curves for the buildup and AFD of (J_{rs}) intersect at the 50% mark [26]. This 50% intersection point should occur when the J_r-acquisition field and the peak AF equal B_{cr}. The Cisowski test is highly diagnostic, because failure of this test most probably indicates that an assemblage either consists of SD particles affected strongly by magnetic interactions, or that it consists of particles which are not homogeneously magnetized SDs. In Fig. 3 it is seen that the <0.1 μm assemblage resoundingly fails this test, despite J_{rs}/J_s being near 0.5. Similarly, the submicron, SD assemblages of magnetite studied by Argyle and Dunlop [27] also fail this test.

Thus, interactions are one explanation for the discrepancy between theoretical predictions and the 'positive' Lowrie–Fuller test for SD behavior often obtained from very fine-grained assemblages. At high temperatures where TRM is acquired and energy barriers are low, the moments of a large percentage of particles could relax easily into the low-energy states that result when nearest-neighbor moments are antiparallel. Over two decades ago, Dunlop and West [28] invoked this mechanism to explain why experimental TRM acquisition curves rise much less steeply with b_{ex} than predicted by Néel's SD theory. In contrast, application of a strong field at room temperature would force nearest-neighbor moments to align and thus assume a metastable configuration. In this second case, most interactions would be 'negative'. As a result, (J_{rs}) would collapse readily under AFD. Nevertheless, J_{rs}/J_s still could be very near or equal to the ideal value of 0.5 for uniaxial anisotropy, if interaction fields triggered few particles to reverse in zero field. According to this scenario, TRM would be more stable to AFD than (J_{rs}), as observed for numerous samples that otherwise display SD-type hysteresis behavior [29–31].

6. Possible role of LEM states

The above discussions of PSD through MD behavior focus on wall–defect interactions and their possible impact on AF demagnetization curves. Also, in the discussions above it is assumed that a particle's number of domain walls is the same for the different states of magnetization and throughout the AFD process. Yet both domain studies [32–34] and micromagnetic models [19,35–39] support the reality of local energy minimum, or LEM, domain states. In particles large enough to energetically favor subdivision into two or more domains, each LEM state is characterized by a certain number of walls. Adjacent LEMs are separated by energy barriers, so that a particle may stably occupy a LEM until exposed to the appropriate external field or heated to sufficiently high temperature. Micromagnetic models also show that defect-free, submicron magnetite particles slightly larger than the classical, SD transition size can occupy SD-like LEM states, such as the vortex state [39]. Transitions between such exotic spin states during hysteresis account reasonably well for hysteresis parameters obtained experimentally from assemblages of <1 μm magnetite grown without a parent matrix [39].

Therefore, field-driven transitions between LEM states provide a mechanism that could profoundly affect AFD behavior. This possibility raises an intriguing question: could a sample's Lowrie–Fuller response reflect differences between the stabilities of LEM states associated, respectively, with weak-field TRM and (J_{rs})? In particles large enough to support walls, for example, the operant stability mechanism would depend on whether most walls unpin in fields which are (1) less than or (2) greater than the fields required for the first LEM–LEM transition. If (1) is true, then wall-unpinning largely controls the stability of a grain in a particular state of remanence. But

if (2) applies, then remanence stability is strongly coupled to transitions among LEM states.

Domain observation studies of titanomagnetite and pyrrhotite provide good evidence that a particle's final LEM state depends on thermomagnetic treatment [32–34]. Thus, such results suggest the idea that the stability mechanism depends on the state of magnetization. If, for example, the LEM state associated with weak-field TRM was much more stable than that associated with (J_{rs}), then (J_{rs}) could demagnetize much more readily than TRM simply through collapse of the initial domain state. This mechanism could apply to particles large enough to subdivide into a classical domain structure, as well as to the very small, inhomogeneously magnetized, but still SD-like particles predicted by micromagnetic theories.

The LEM states that characterize weak-field TRM and (J_{rs}) have yet to be determined experimentally for magnetite particles of various grain sizes and provenance. More important, the critical links among LEM states, remanent intensity, bulk stability, and thermomagnetic state have not been investigated deeply in any magnetic material, let alone those of paleomagnetic importance. The possible impact of LEM–LEM transitions on AFD behavior remains a fascinating but unsolved problem that requires much future experimental work.

7. Summary and conclusions

Assemblages of glass–ceramic (GC) magnetite that encompass single-domain (SD) through truly multidomain (MD) hysteresis behavior all acquire weak-field TRMs which are more stable to alternating field demagnetization (AFD) than (J_{rs}). In the case of truly MD assemblages this result is especially surprising. Because the GC method of synthesis is thought to produce high dislocation densities, Xu and Dunlop's model [13] would lead one to predict a MD-like Lowrie–Fuller response from the coarsest-grained assemblage studied here, whose average grain size is approximately 100 μm. Because this prediction is not fulfilled, Xu and Dunlop's model requires close theoretical scrutiny and careful experimental testing.

Even the AFD responses of supposedly SD assemblages pose interesting questions about observations versus theory. Although submicron GC magnetites exhibit J_{rs}/J_s-values near 0.5 and yield SD-like Lowrie–Fuller tests, they fail the 'Cisowski' test for noninteracting SD grains. Here, it is shown theoretically that assemblages of noninteracting, uniaxial SD grains should respond in just the opposite sense to that stated by the Lowrie–Fuller test for the SD state. Magnetic interactions could resolve these apparent conflicts; if this interpretation is correct, then SD magnetite assemblages synthesized with the GC method could be more strongly affected by interactions than previously thought.

However, we also propose that AF demagnetization characteristics could reflect the dependence of a particle's LEM state — and its resultant stability — on the particular state of magnetization. This mechanism not only could apply to PSD and truly MD grains, but also to SD-like grains capable of occupying a number of spin configurations, such as the vortex state. This scenario will remain intriguing but speculative, until domain studies address the dependence of LEMs on different thermomagnetic treatments.

Acknowledgements

The author extends her thanks to Robert Kamau for his help in measuring the samples studied here, and to Andrew Newell and Lisa Tauxe for their helpful reviews. This work was supported by NSF grant EAR94-18405. ***[RV]***

Appendix A

Histograms of the grain-size distributions obtained in the SEM for the five glass–ceramic magnetite assemblages studied here.

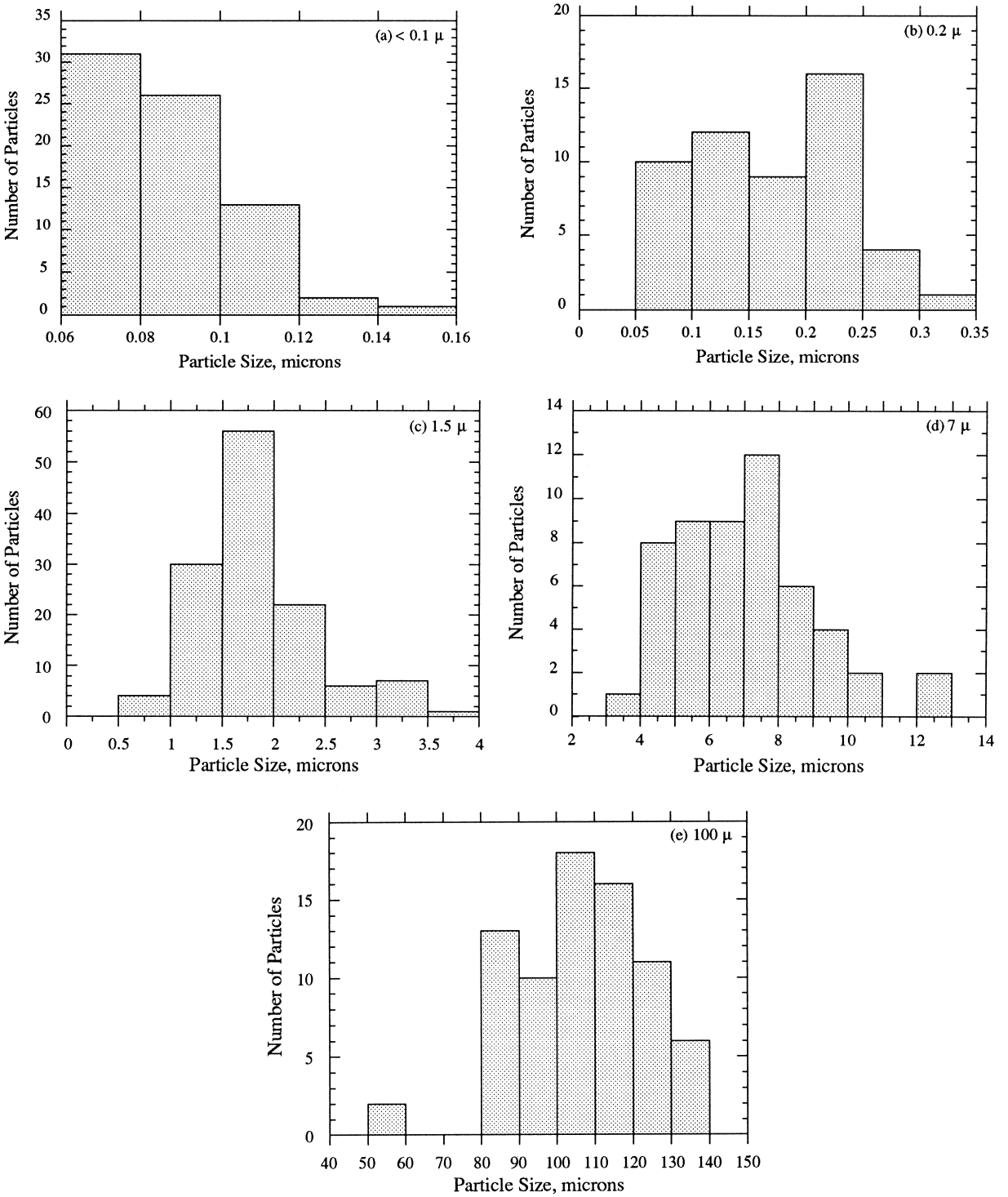

Appendix B

We assume a simple model of homogeneously magnetized, uniaxial, aligned, noninteracting SD grains, whose intrinsic properties are numerically equal to those of magnetite. It is assumed that all applied fields are parallel to the particles' easy axes. B_c is the critical field required to flip a particle's magnetization through 180º.

For shape anisotropy, $B_c = \Delta N M_s$, where ΔN is the demagnetizing factor and M_s equals spontaneous magnetization at temperature T. In magnetite at room temperature T_o, $M_{so} \cong 4.8 \times 10^5$ A/m (SI) or 480 emu/cm^3 (cgs) [23]. Because $\Delta N_{max} = 2\pi$, we have set $B_{co,max} \cong 301.6$ mT (3.016×10^3 Oe). Because it is assumed that uniaxial anisotropy outweighs cubic magnetocrystalline anisotropy, $B_{co,min}$ is set equal to $2|K_1|/M_{so} = 56.2$ mT (562 Oe), where K_1 is the first magnetocrystalline anisotropy constant of magnetite ($\cong -1.35 \times 10^4$ J/m^3; -1.35×10^5 erg/cm^3) [23].

For uniaxial stress anisotropy, $B_{co} = 3/2\lambda_o\sigma/M_{so}$, where λ_o = magnetostriction constant at room temperature T_o and σ = stress. In magnetite, $\lambda_o \cong 4 \times 10^{-5}$ [23–25]. If σ_{max} is on the order of the breaking strength of magnetite ($\cong 1-2\times 10^9$ N/m^2; 1–2 $\times 10^{10}$ dyne/cm^2) [40], then $B_{co,max} \cong 200$ mT (2×10^3 Oe).

In uniaxial SD grains, the temperature dependence of critical field is given by $B_c = B_{co}m^p \propto K_u/M_s$, where $m = M_s/M_{so}$, K_u is the uniaxial anisotropy energy density constant at temperature T, and M_s is spontaneous magnetization at T. In GC magnetite, $m \cong [(T_c - T)/(T_c - T_o)]^{0.43}$, where T_c is the Curie point ($\cong$853 K) [41]. The power p depends on the source of anisotropy. For shape anisotropy, $p = 1$, exactly. For stress anisotropy, $\lambda \propto m^{2.25}$ to m^3, so that $p \cong 1.25$ to 2 [24,25]; $p = 2$ was used in this model. As reported by Worm et al. [41], in SD, GC magnetite the temperature dependence of B_c indicates a large contribution from stress.

References

[1] H.-Ü. Worm, Herstellung und magnetische Eigenschaften kleiner Titanomagnetit-Ausscheidungen in Silikaten, Ph.D. thesis, Universitat Bayreuth, 1986, 163 pp.

[2] H.-Ü. Worm, H. Markert, The preparation of dispersed titanomagnetite particles by the glass–ceramic method, Phys. Earth Planet. Inter. 46 (1987) 263–269.

[3] H.-Ü. Worm, H. Markert, Magnetic hysteresis properties of fine particle titanomagnetites precipitated in a silica matrix, Phys. Earth Planet. Inter. 46 (1987) 84–92.

[4] C.P. Hunt, B.M. Moskowitz, S.K. Banerjee, in: Magnetic Properties of Rocks and Minerals, Rock Physics and Phase Relations: a Handbook of Physical Constants, AGU Ref. Shelf 3 (1995), 189–204.

[5] F. Heider, D.J. Dunlop, N. Sugiura, Magnetic properties of hydrothermally recrystallized magnetite crystals, Science 236 (1987) 1287–1290.

[6] D.J. Dunlop, Hysteresis properties of magnetite and their dependence on particle size: a test of pseudo-single-domain remanence models, J. Geophys. Res. 91B (1986) 9569–9584.

[7] D.J. Dunlop, K.S. Argyle, Separating multidomain and single-domain-like remanences in pseudo-single-domain magnetites (215–540 nm) by low-temperature demagnetization, J. Geophys. Res. 96 (1991) 2007–2017.

[8] W. Lowrie, M. Fuller, On the alternating field demagnetization characteristics of multidomain thermoremanent magnetization in magnetite, J. Geophys. Res. 76 (1971) 6339–6349.

[9] F. Rimbert, Contribution à l'étude de l'action de champs alternatifs sur les aimantations rémanentes des roches, Applications géophysiques, Rev. Inst. Fr. Pét. Ann. Combust. Liq. 14 (1959) 17–54, 123–155.

[10] H.P. Johnson, W. Lowrie, D.V. Kent, Stability of anhysteretic remanent magnetization in fine and coarse magnetite and maghemite particles, Geophys. J. R. Astron. Soc. 41 (1975) 1–10.

[11] M.E. Bailey, D.J. Dunlop, Alternating field characteristics of pseudo-single-domain (2–14 μm) and multidomain magnetite, Earth Planet. Sci. Lett. 63 (1983) 335–352.

[12] D.J. Dunlop, Determination of domain structure in igneous rocks by alternating field and other methods, Earth Planet. Sci. Lett. 63 (1983) 353–367.

[13] S. Xu, D.J. Dunlop, Toward a better understanding of the Lowrie–Fuller test, J. Geophys. Res. 100 (1995) 22533–22542.

[14] W. Williams, The Effect of Time and Temperature on Magnetic Remanence, Ph.D. thesis, Cambridge University, 1986, 140 pp.

[15] S.L. Halgedahl, R.D. Jarrard, Low-temperature behavior of single-domain through multidomain magnetite, Earth Planet. Sci. Lett. 130 (1995) 127–139.

[16] S.L. Halgedahl, Experiments to investigate the origin of anomalously elevated unblocking temperatures, J. Geophys. Res. 98 (1993) 22443–22460.

[17] F. Heider, D.J. Dunlop, H.C. Soffel, Low-temperature and alternating field demagnetization of saturation remanence and thermoremanence in magnetite grains (0.037 μm to 5 mm), J. Geophys. Res. 97 (1992) 9371–9381.

[18] B.M. Moskowitz, Micromagnetic study of the influence of crystal defects on coercivity in magnetite, J. Geophys. Res. 98 (1993) 18011–18026.

[19] T. Moon, R.T. Merrill, The magnetic moments of nonuniformly magnetized grains, Phys. Earth Planet. Inter. 34 (1984) 186–194.

[20] L. Néel, Théorie du traînage magnétique des ferromagnétiques en grains fins avec applications aux terres cuites, Ann. Géophys. 5 (1949) 99–136.

[21] L. Néel, Some theoretical aspects of rock magnetism, Adv. Phys. 4 (1955) 191–242.

[22] V.A. Schmidt, The variation of the blocking temperature in models of thermoremanence (TRM), Earth Planet. Sci. Lett. 29 (1976) 146–154.

[23] Y. Syono, Magnetocrystalline anisotropy and magnetostric-

tion of Fe_3O_4–Fe_2TiO_4 series, with special applications to rock magnetism, Jpn. J. Geophys. 4 (1965) 71–143.
[24] G.D. Klapel, P.N. Shive, High-temperature magnetostriction of magnetite, J. Geophys. Res. 79 (1974) 2629–2633.
[25] B.M. Moskowitz, High-temperature magnetostriction of magnetite and titanomagnetite, J. Geophys. Res. 98B (1993) 359–371.
[26] S. Cisowski, Interacting vs. non-interacting single domain behavior in natural and synthetic samples, Earth Planet. Sci. Lett. 26 (1982) 56–62.
[27] K.S. Argyle, D.J. Dunlop, Low-temperature and high-temperature hysteresis of small multidomain magnetites (215–540 nm), J. Geophys. Res. 95 B5 (1990) 7069–7083.
[28] D.J. Dunlop, G.F. West, An experimental evaluation of single domain theories, Rev. Geophys. 7 (1969) 709–757.
[29] Ö. Özdemir, W. O'Reilly, An experimental study of the intensity and stability of thermoremanent magnetization acquired by synthetic monodomain titanomagnetite substituted by aluminum, Geophys. J. R. Astron. Soc. 70 (1982) 141–154.
[30] Ö. Özdemir, High-temperature hysteresis and thermoremanence of single-domain maghemite, Phys. Earth Planet. Inter. 65 (1990) 125–136.
[31] D.J. Dunlop, S. Xu, Ö. Özdemir, D. AlMawlawi, M. Moskovits, Magnetic properties of arrays of oriented iron particles as a function of particle size, shape and spacing, Phys. Earth Planet. Inter. 76 (1993) 113–121.
[32] S.L. Halgedahl, M. Fuller, The dependence of magnetic domain structure upon magnetization state with emphasis upon nucleation as a mechanism for pseudo-single-domain behavior, J. Geophys. Res. 88 (1983) 6505–6522.
[33] F. Heider, S.L. Halgedahl, D.J. Dunlop, Temperature dependence of magnetic domains in magnetite crystals, Geophys. Res. Lett. 15 (1988) 184–187.
[34] S.L. Halgedahl, Magnetic domain patterns observed on synthetic Ti-rich titanomagnetite as a function of temperature and in states of thermoremanent magnetization, J. Geophys. Res. 96 (1991) 3943–3972.
[35] W. Williams, D.J. Dunlop, Three-dimensional modelling of ferromagnetic domain structure, Nature 337 (1989) 634–637.
[36] W. Williams, D.J. Dunlop, Some effects of grain shape and varying external magnetic fields on the magnetic structure of small grains of magnetite, Phys. Earth Planet. Inter. 65 (1990) 1–14.
[37] A.J. Newell, D.J. Dunlop, W. Williams, A two-dimensional micromagnetic model of magnetizations and fields in magnetite, J. Geophys. Res. 98 (1993) 9553–9559.
[38] D.J. Dunlop, A.J. Newell, R.J. Enkin, Transdomain thermoremanent magnetization, J. Geophys. Res. 99 (1994) 19741–19755.
[39] W. Williams, D.J. Dunlop, Simulation of magnetic hysteresis in pseudo-single-domain grains of magnetite, J. Geophys. Res. 100 (1995) 3859–3871.
[40] C.R. Barrett, W.D. Nix, A.S. Tetelman, The Principles of Engineering Materials, Prentice-Hall, Englewood Cliffs, NJ, 1973.
[41] H.-Ü. Worm, M. Jackson, P. Kelso, S.K. Banerjee, Thermal demagnetization of partial thermoremanent magnetization, J. Geophys. Res. 93 (1988) 12196–12204.